Desalination and Water Treatment
www.deswater.com

doi: 10.5004/dwt.2021.27381

229 (2021) 384–394
July

An investigation of natural and modified diatomite performance for adsorption of Basic Blue 41: isotherm, kinetic, and thermodynamic studies

Ali Rıza Kul[a], Adnan Aldemir[b,*], Hülya Koyuncu[c]

[a]*Chemistry Department, Faculty of Science, Van Yüzüncü Yıl University, 65080 Van, Turkey, email: alirizakul@yyu.edu.tr*
[b]*Chemical Engineering Department, Faculty of Engineering, Van Yüzüncü Yıl University, 65080 Van, Turkey, email: adnanaldemir@yyu.edu.tr*
[c]*Chemical Engineering Department, Faculty of Engineering and Natural Sciences, Bursa Technical University, 16310 Bursa, Turkey, email: hulya.koyuncu@btu.edu.tr*

Received 2 March 2021; Accepted 29 April 2021

ABSTRACT

In the present study, natural diatomite (ND) and Mn-modified diatomite (MD) were utilized for adsorption of Basic Blue 41 (BB 41) from aqueous solution at temperatures of 298, 308, and 318 K. Based on the results of isotherm studies, the Freundlich isotherm model is better than the Langmuir and Temkin models. Isotherm constants increase as the temperature increases, indicating that the removal process is favorable at higher temperatures. Adsorption kinetics for BB 41 on diatomite best fit the pseudo-second-order model which had kinetic constants that were higher than pseudo-first-order and intra-particle diffusion models. When the initial dye concentration rises from 10 to 80 mg L^{-1}, adsorption capacity on ND and MD increase from 6.15 to 62.43 mg g^{-1} and 9.06 to 75.95 mg g^{-1} at 318 K, respectively. Gibbs free energy ($\Delta G°$) values for BB 41 adsorption on ND and MD were determined as –11.224 and –15.586 kJ mol^{-1} at 318 K, respectively. Enthalpy ($\Delta H°$) values for this removal process were calculated as 31.746 and 48.706 kJ mol^{-1}, with entropy ($\Delta S°$) values determined as 133.319 and 170.728 J mol^{-1} K^{-1} for ND and MD, respectively. Activation energy (E_A) values were determined as 42.7 and 58.83 kJ mol^{-1} for BB 41 removal onto ND and MD adsorbents, respectively. Economic analysis of the preparation of Mn-modified diatomite was carried out. The results indicate that diatomite could be a good material compared to more costly adsorbents used for dye removal.

Keywords: Adsorption; Basic Blue 41; Diatomite; Isotherm; Kinetic; Thermodynamic

1. Introduction

Over recent decades, the more industrial production progresses, the more dyes are widely utilized in various industries [1]. Because of their high density [2], powerful toxicity [3], and poor biodegradability [4], dyes are preserved in water for long periods endangering the biodiversity of aquatic ecosystems [5], harming ecological balances, and even putting the lives of animate objects and humans in danger [6]. Various techniques are used individually or in combination for the removal of dyes from wastewater today [7,8]. Among these methods, adsorption is recommended by experts because of its energy efficiency, effectiveness, being free of secondary pollution, and low costs for treatment of wastewater [9–11].

Different kinds of adsorbents are utilized for the treatment of dye-contaminated wastewater [12]. Activated carbon is a common adsorbent for the isolation of dyes thanks to its high removal capacity. Yet, its industrial application is limited due to its disadvantages, such as costliness and easy

* Corresponding author.

desorption. Thus, natural adsorbents like clays and waste materials are applied because they are less costly and ecologically friendly [13]. Diatomite is a material mainly made up of siliceous particulates [14,15]. Diatomite has unique features since it has a very high surface area and porous structure, high stability, and rather low density [16,17]. Thus, it is utilized as an adsorbent, support, and filtration material, in agrarian and pharmaceutic applications [18,19]. Diatomite is widely used as an adsorbent for the adsorption of toxic contaminants with high removal percentages [20,21]. This research aims to investigate the performance of natural diatomite and Mn-modified diatomite for removal of Basic Blue 41 (BB 41) from aqueous solutions, including isotherm, kinetic, and thermodynamic studies.

2. Materials and methods

2.1. Preparation of adsorbent (natural and Mn-modified diatomite)

All chemicals were purchased with analytical purity and used without purification. Distilled water was used in all experiments. The adsorption experiments were carried out with natural and Mn-modified diatomite adsorbents. Natural diatomite was obtained as a resource from the Çaldıran region of Van, Turkey. For modification of natural diatomite, a reactor made of pyrex glass with a condenser was used. Then 15 g diatomite was mixed with 6 M NaOH at 80°C for 2 h. $MnCl_2$ was added to this mixture and mixed for 12 h at room temperature by adjusted its pH to 2 with 6 M HCl. The diatomite was remixed with 6 M NaOH at room temperature for 12 h to accelerate the MnOH formation rate, and the mixture was left in the air for oxidation. The prepared adsorbent was washed with distilled water before being dried in an oven at 100°C for 24 h. As the last process, it was powdered by pounding in a porcelain mortar and stored in plastic tubes for use in experiments.

The characterization of natural and modified diatomite samples was carried out with instrumental techniques. Chemical analysis of diatomite samples was obtained by an X-ray fluorescence spectrometer (Philips 2400) and pore size distributions of diatomite samples were recorded with X-ray diffractograms (Philips PW 1830-40). Thermal analysis was carried out using a thermal analyzer (TG-DTA, Rigaku 2.22E1) and infrared measurements have performed a spectrophotometer (Fourier-transform infrared (FT-IR), Bio-Rad Win-IR). Details of the characterization results for natural and modified diatomite were given in previous publications by the authors. XRD spectrogram indicates that the diatomite consists mainly of silica (SiO_2) with smaller amounts of Al_2O_3, Fe_2O_3, TiO_2, Na_2O, and K_2O. According to FT-IR analysis, it was observed that OH bands disappeared after modification [22–24].

2.2. Adsorbate (Basic Blue 41)

The cationic dye BB 41 was used as the adsorbate in the current research. The formula of BB 41 is $C_{20}H_{26}N_4O_6S_2$ (MW 482.57 g mol^{-1}) which was procured from Sigma-Aldrich Company and used without any purification. A stock solution was prepared by dissolving the required dye amount in distilled water. For batch experiments 10, 20, 30, 40, 50, 60, 70, and 80 mg L^{-1} solutions of BB 41 dye were prepared with deionized water using the stock dye solution.

2.3. Adsorption experiments

In batch experiments which were completed in a temperature-controlled water bath (Julabo, EC-13A), the prepared adsorbent was treated with 500 mL of dye solution. All experiments were performed at pH 5.5 and 1 g of adsorbent mass was used for treatment because the highest removal (%) was obtained with these values. The pH values of solutions were adjusted to pH 5.5 by adding negligible volumes of 0.1 N HCl and 0.1 N NaOH solutions with a pH meter (Selecta, pH-2005). BB 41 concentration in the dye solution was determined for 240 min. The suspension was centrifuged (Nüve, NF800) at 5,000 rpm for 10 min and the supernatant was analyzed for residual BB 41 concentration by spectrophotometer (PG Instruments, T80/T80+) at 617 nm wavelength. All experiments were performed in duplicate in the same conditions, which were 298, 308, and 318 K temperatures and the average of the obtained data was taken as the result. The unknown BB 41 concentrations were determined with a calibration curve which was obtained by plotting absorbance and different dye concentrations. The dye adsorption capacity on the adsorbent was calculated with Eq. (1):

$$q_e = \frac{\left(C_0 - C_e\right)V}{m} \tag{1}$$

where V symbolizes solution volume (L), C_0 and C_e represent initial and equilibrium concentration of dye (mg L^{-1}), and m denotes adsorbent mass (g). The dye removal percentage was determined with Eq. (2):

$$\text{Dye removal efficiency}\left(\%\right) = \frac{\left(C_0 - C_t\right)}{C_0} \times 100 \tag{2}$$

Ultimately, data obtained from this study were tested by fitting the isotherm, kinetic, and thermodynamic relationships for BB 41 dye removal using natural and modified diatomite.

2.4. Adsorption isotherm studies

The Freundlich, Langmuir, and Temkin isotherms were used to explain the interaction of adsorbate molecules and adsorbent surface. Both models were applied for the description of the experimental data obtained at three temperatures. The Langmuir model assumes the adsorption occurs on a homogenous surface with no interactions between adsorbates on the plane of the surface and its equation is given in Eq. (3):

$$q_e = \frac{\left(q_m K_L C_e\right)}{\left(1 + K_L C_e\right)} \tag{3}$$

where q_m denotes maximum adsorption capacity (mg g^{-1}), K_L is Langmuir constant (L g^{-1}). q_m and K_L can be determined from the slope and intercept of the straight line which is obtained by plotting C_e/q_e vs. C_e [25]. The dimensionless separation factor (R_L) can be obtained from Eq. (4):

$$R_L = \frac{1}{1 + K_L C_e} \tag{4}$$

where R_L of $0 < R_L < 1$ indicates favorable adsorption. The Freundlich isotherm is an empirical model based on adsorption occurring on a heterogeneous surface and its equation is given in Eq. (5):

$$q_e = K_F C_e^{1/n} \tag{5}$$

where K_F is the Freundlich constant (L g^{-1}), and n is an empirical coefficient. A straight line was obtained for the plot of the natural logarithm of q_e vs. C_e. The slope and intercept of the line give n and K_F values, respectively [26]. The Temkin isotherm describes the concept that the heat of adsorption decreases on covering a solid surface [27]. The Temkin equation used for the determination of isotherm parameters is given with Eq. (6):

$$q_e = B \ln\left(K_T C_e\right) \tag{6}$$

where K_T is a constant substitute for the maximum binding energy and B is related to the heat of adsorption. B values are calculated with Eq. (7):

$$B = \frac{RT}{b_T} \tag{7}$$

where $1/b_T$ indicates the adsorption potential of adsorbent, R is gas constant (8.314 kJ mol^{-1}), and T is the temperature (K). Langmuir, Freundlich, and Temkin isotherm results for BB 41 adsorption on natural and Mn-modified diatomite at 318 K are given in Figs. 1–3, respectively. Isotherm parameters for the Langmuir, Freundlich, and Temkin models are given in Table 1 and comparisons of BB 41 adsorption capacities with different adsorbents are given in Table 2.

2.5. Adsorption kinetic studies

In this study, the BB 41 adsorption data were analyzed by pseudo-first-order (PFO), pseudo-second-order (PSO), and intra-particle diffusion (IPD) kinetic models. Adsorption experiments were conducted with eight initial concentrations of BB 41, viz. 10, 20, 30, 40, 50, 60, 70, and 80 mg L^{-1}, respectively. The amounts of BB 41dye molecules adsorbed at various time periods (q_t) were calculated with Eq. (8):

$$q_t = \frac{\left(C_0 - C_t\right)V}{m} \tag{8}$$

where C_t is the concentration of BB 41 dye molecules present in an aqueous solution after t min. The most well-suited model was determined based on correlation coefficient (R^2) values. Lagergren's equation may be the first for describing adsorption kinetics based on solid capacity and this equation is called the PFO kinetic model [28]. The PFO kinetic model equation is given in Eq. (9):

$$\ln\left(q_e - q_t\right) = \ln q_e - k_1 t \tag{9}$$

where k_1 (min^{-1}) is the rate constant of this kinetic model. In order to obtain the constants in this model, the plot of $\ln(q_e - q_t)$ against t is drawn. The PSO kinetic model explains chemical bond formation between adsorbent and solute molecules based on adsorption capacity [29]. The PSO kinetic model is given with Eq. (10):

$$\frac{t}{q_t} = \frac{1}{\left(k_2 q_e^2\right)} + \frac{t}{q_e} \tag{10}$$

where k_2 represents the adsorption rate constant (g mg^{-1} min^{-1}). k_2 and q_e values were identified from the plot of t/q_t vs. t. The IPD kinetic model was proposed by Weber and Morris [30] and tests the possibility of IPD as a rate-limiting step using the IPD model which is given in Eq. (11):

$$q_t = k_{\text{ipd}} t^{0.5} + C \tag{11}$$

where k_{ipd} (mg g^{-1} min$^{-1/2}$) is rate constant and C is boundary thickness constant. A plot of q_t against $t^{0.5}$ at different BB 41 concentrations gave two phases of linear plots. PFO, PSO, and IPD kinetic parameters for BB 41 adsorption on natural and Mn-modified diatomite are given in Table 3 for 80 mg L^{-1} initial BB 41 concentration.

2.6. Adsorption thermodynamic studies

Gibbs free energy ($\Delta G°$), enthalpy ($\Delta H°$), and entropy ($\Delta S°$) parameters are significant to determine heat changes during the adsorption process between adsorbate and adsorbent. These parameters are determined with equations shown in Eqs. (12)–(14):

$$\Delta G° = -RT \ln K_d \tag{12}$$

$$\Delta G° = \Delta H° - T\Delta S° \tag{13}$$

$$\ln K_d = \frac{\Delta S°}{R} - \frac{\Delta H°}{RT} \tag{14}$$

where K_d is the thermodynamic constant (L g^{-1}), obtained by plotting q_e/C_e vs. q_e. $\Delta H°$ and $\Delta S°$ parameters are calculated from the plot of $\ln K_d$ vs. $1/T$. Thermodynamic parameters are illustrated in Table 4. The activation energy (E_A) provides an idea about the type of adsorption, such as physical (0–40 kJ mol^{-1}) or chemical adsorption (40–800 kJ mol^{-1}). E_A values for this process are calculated from the Arrhenius equation which is given with Eq. (15):

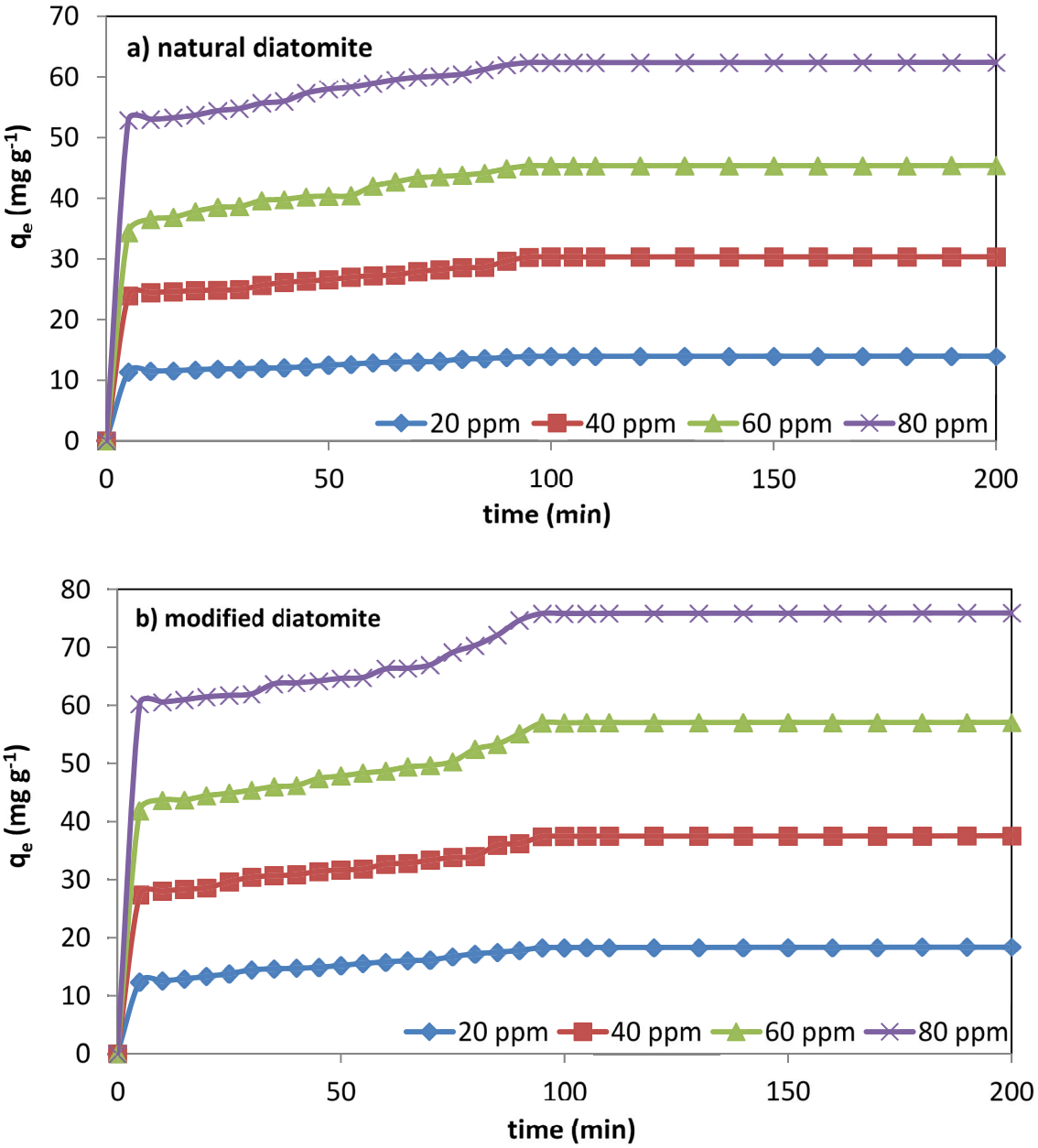

Fig. 1. Effect of initial concentration for adsorption of BB 41 at 318 K: (a) natural diatomite and (b) Mn modified diatomite.

$$\ln k_2 = \ln A - \frac{E_A}{RT} \tag{15}$$

where k_2 is adsorption rate constant (g mol^{-1} s^{-1}), A is the Arrhenius factor (g mol^{-1} s^{-1}), E_A is activation energy (J mol^{-1}), R is gas constant (J mol^{-1} K^{-1}), and T is adsorption temperature (K).

3. Results and discussion

3.1. Effect of contact time and initial dye concentrations

Contact time and initial concentrations plots of BB 41 adsorption at 298 K are shown in Figs. 1a and b for natural diatomite and Mn-modified diatomite, respectively. Fig. 1 is shown in the experimental adsorption capacity q_e (mg g^{-1}) as a function of contact time and these curves are explained that BB 41 adsorption speed is very high for the first period and remains constant after 100 min indicating an equilibrium. Indeed, this can be explained by the fact that the migration of the dye solution can easily accessible to the vacant sites of the adsorbent in the initial period. Thus a higher adsorption percentage is a result of the gradient concentration of the solid–liquid interface. The gradient concentration is extremely high at the beginning of contact between the solid and liquid phases. However, in the next period adsorption decreases due to the slower diffusion of the dissolved species through the adsorbent pores. The rapid removal of

dyes facilitates the use of the decreased adsorbent volumes and thus ensures the efficiency and cost of the process operation.

As the initial BB 41 concentration increased from 10 to 80 mg L^{-1}, the BB 41 adsorption capacity on the natural and Mn modified diatomite increased from 6.15 to 62.43 mg g^{-1} and 9.06 to 75.95 mg g^{-1} for 318 K, respectively. These data prove that the initial dye concentration plays a crucial role in dye adsorption capacity and provides a driving power in the interaction between the adsorbent and the dye. After batch experiments, 69.86%, 77.02%, and 78.06% removal percentages were achieved with natural diatomite for 80 mg L^{-1} initial dye concentration at 298, 308, and 318 K, respectively. Comparatively, 85.04%, 90.69%, and 94.94% removal percentages were obtained with modified diatomite for 80 mg L^{-1} initial dye concentration at 298, 308, and 318 K, respectively. According to the results, Mn-modified diatomite provides a higher removal capacity than natural diatomite for adsorption of BB 41.

3.2. Adsorption isotherm results of BB 41 on diatomite

The Freundlich, Langmuir, and Temkin models were chosen to explain the interaction of adsorbate molecules and adsorbent surfaces in this study. All models were applied for the description of the experimental data obtained at three temperatures. The coefficients of these isotherm models determined for adsorption of BB 41 on ND and MD are presented in Table 1. With respect to the coefficients, the Freundlich model fits better than the Langmuir and Temkin isotherm models. The values of K_F and n increase as temperature increases, and also indicate that adsorption is more favorable at the higher temperature. R^2 values for the Freundlich model were higher than Langmuir and Temkin model values. The n values were determined from the Freundlich isotherm and these values were higher than 1.0 for ND and MD which indicates good adsorption by this adsorbent and high efficiency of the Mn modification [22]. Freundlich isotherm plots of BB 41 adsorption on natural diatomite and Mn-modified diatomite at 318 K are shown in Fig. 2.

Monolayer adsorption capacity (q_m) values were determined as 56.82 and 85.64 mg g^{-1} for ND and MD at 318 K, respectively. The adsorption intensity (K_L) values were obtained as 0.0149 and 0.0225 L mg^{-1} for ND and MD at 298 K, respectively. The separation factor (R_L) values for ND and MD were determined as 0.74 and 0.79, respectively, which indicate favorable adsorption. Langmuir isotherm plots of BB 41 adsorption on natural diatomite and Mn-modified diatomite at 318 K are shown in Fig. 3.

The Temkin constants (K_T) values, which are related to the maximum binding energy, were determined as 0.2379 and 0.4961 L g^{-1} for ND and MD at 298 K, respectively. b_T values that represent the heat of adsorption were defined as 180.029 and 161.859 J mol^{-1} for ND and MD at 298 K, respectively. It is noted that the K_T values increase as temperature increases, and b_T values decrease as temperature increases. Temkin isotherm plots of BB 41 adsorption on natural diatomite and Mn-modified diatomite at 318 K are shown in Fig. 4.

Various studies in the literature have investigated the usage of different adsorbents and biosorbents for BB 41 adsorption. A comparison of the monolayer adsorption capacity of BB 41 by various adsorbents is given in Table 2. As it is evident, diatomite has the highest removal capacity after rich tuff for adsorption of BB 41 dye from aqueous solutions. When the results of case studies and those of the present study are compared that BB 41 adsorption capacity of diatomite is good and it can be used for dye removal as an inexpensive adsorbent. Also, according to the results, Mn-modified diatomite provides a higher removal capacity than natural diatomite for adsorption of BB 41.

3.3. Adsorption kinetic results of BB 41 on diatomite

Kinetic parameters of the PFO, PSO, and IPD models for BB 41 adsorption on ND and MD are given in Table 3. The k_1 and q_e values determined from the plot of $\ln(q_e - q_t)$ against t according to the PFO model are given in Fig. 5a. q_e and k_2 kinetic rate constants were obtained from the plot of t/q_t vs. t for the PSO model which is given in Fig. 5b. k_{ipd} kinetic rate constants and C constants were calculated from slope and intercept of q_t against $t^{0.5}$ for the IPD model which is given in Fig. 5c. It can be observed that the parameters of PFO and IPD kinetic models are lower than the PSO kinetic model; thus, these models are not rate-limiting steps. Results indicate that R^2 coefficients are the highest with q_e values calculated by the process that fits the PSO model. These results suggest that the adsorption process is chemical adsorption. Usually, kinetic data for adsorption is better represented by a PSO model for most dye removal systems [44]. Experimental and calculated q_e values of 318 K were higher than 298 and 308 K values. According to the results, it is obvious that q_e values increased with increasing temperature (Table 3). Kinetic results show that BB 41 adsorption on diatomite abides by the PSO model and suggests that the rate-limiting step is explained by electron exchanges between the diatomite and BB 41 molecules. Also, the values of q_e and kinetic constants determined using PFO, PSO, and IPD models increase as temperature i ncrease [45,46].

3.4. Adsorption thermodynamic results for BB 41 on diatomite

Thermodynamic parameters for BB 41 adsorption onto natural and Mn modified diatomite were calculated using Eqs. (12)–(14) and Gibbs free energy ($\Delta G°$), enthalpy ($\Delta H°$), and entropy ($\Delta S°$) values are given in Table 4. The values obtained for $\Delta G°$ and $\Delta H°$ can help in describing the mechanism of the adsorption process. Thermodynamic parameters for BB 41 adsorption onto modified diatomite are higher than for natural diatomite. $\Delta G°$ values of BB 41 adsorption on ND and MD were determined as –11.224 and –15.586 kJ mol^{-1} for 318 K, respectively. $\Delta H°$ values of BB 41 removal with ND and MD were calculated as 31.746 and 48.706 kJ mol^{-1} with $\Delta S°$ values for this process determined as 133.319 and 170.728 J mol^{-1} K^{-1} for ND and MD, respectively. The negative $\Delta G°$ values, which varied between 0 and –30 kJ mol^{-1}, show the feasibility of this removal process and the spontaneous nature of BB 41

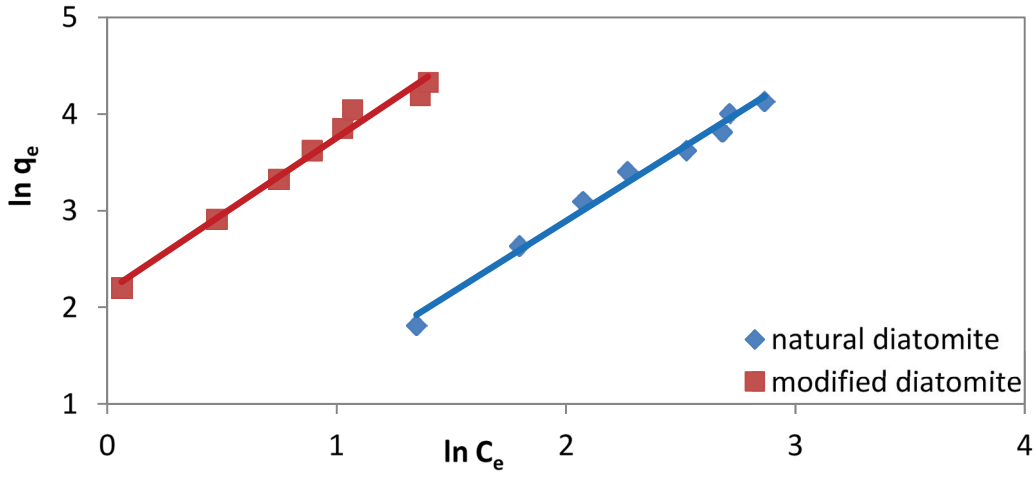

Fig. 2. Freundlich plots of BB 41 adsorption on natural and modified diatomite at 318 K.

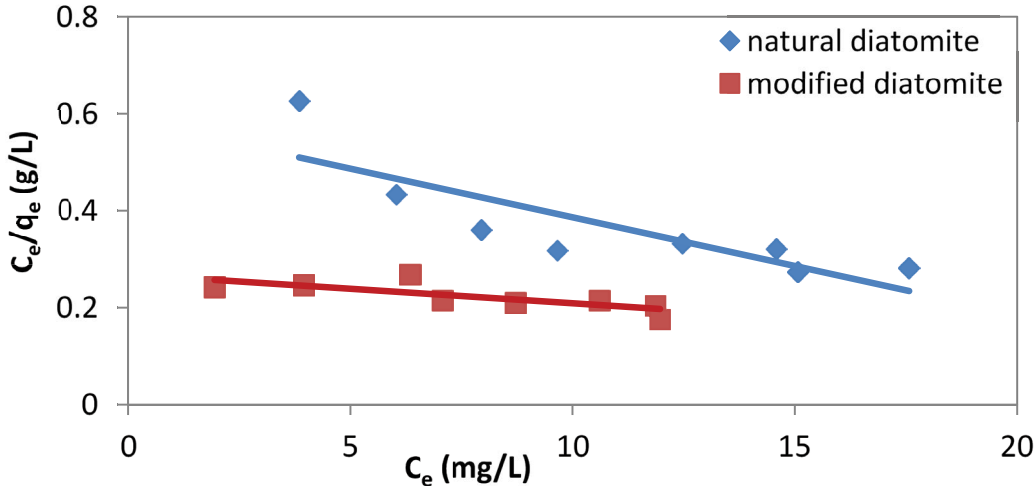

Fig. 3. Langmuir plot of BB 41 adsorption on natural and modified diatomite at 318 K.

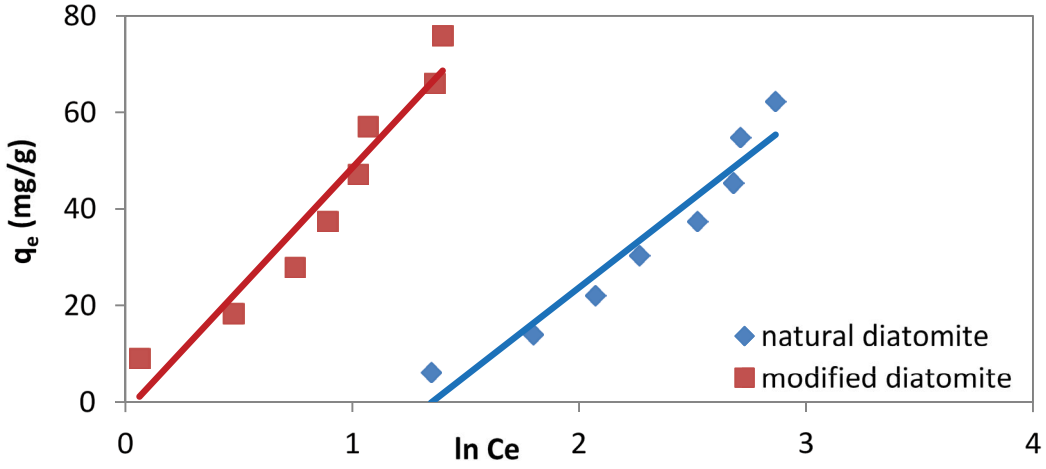

Fig. 4. Temkin plot of BB 41 adsorption on natural and modified diatomite at 318 K.

Table 1
Isotherm model constants for BB 41 adsorption on natural and modified diatomite

	Temperature	Langmuir			Freundlich			Temkin		
	K	K_L (L g^{-1})	q_m (mg g^{-1})	R^2	n	K_F (L g^{-1})	R^2	K_T (L g^{-1})	b_T (J mol^{-1})	R^2
ND	298	0.0085	34.636	0.529	1.673	1.3822	0.986	0.2379	180.029	0.9422
	308	0.0148	45.249	0.787	1.781	1.4583	0.985	0.2401	143.787	0.8954
	318	0.0178	56.821	0.702	1.877	1.5749	0.988	0.2588	124.559	0.9308
MD	298	0.0143	66.679	0.589	1.734	3.4677	0.982	0.4961	161.859	0.8441
	308	0.0221	72.286	0.887	2.348	4.6973	0.981	0.6547	140.969	0.8235
	318	0.0414	85.645	0.784	4.351	8.7007	0.982	0.9616	104.744	0.9337

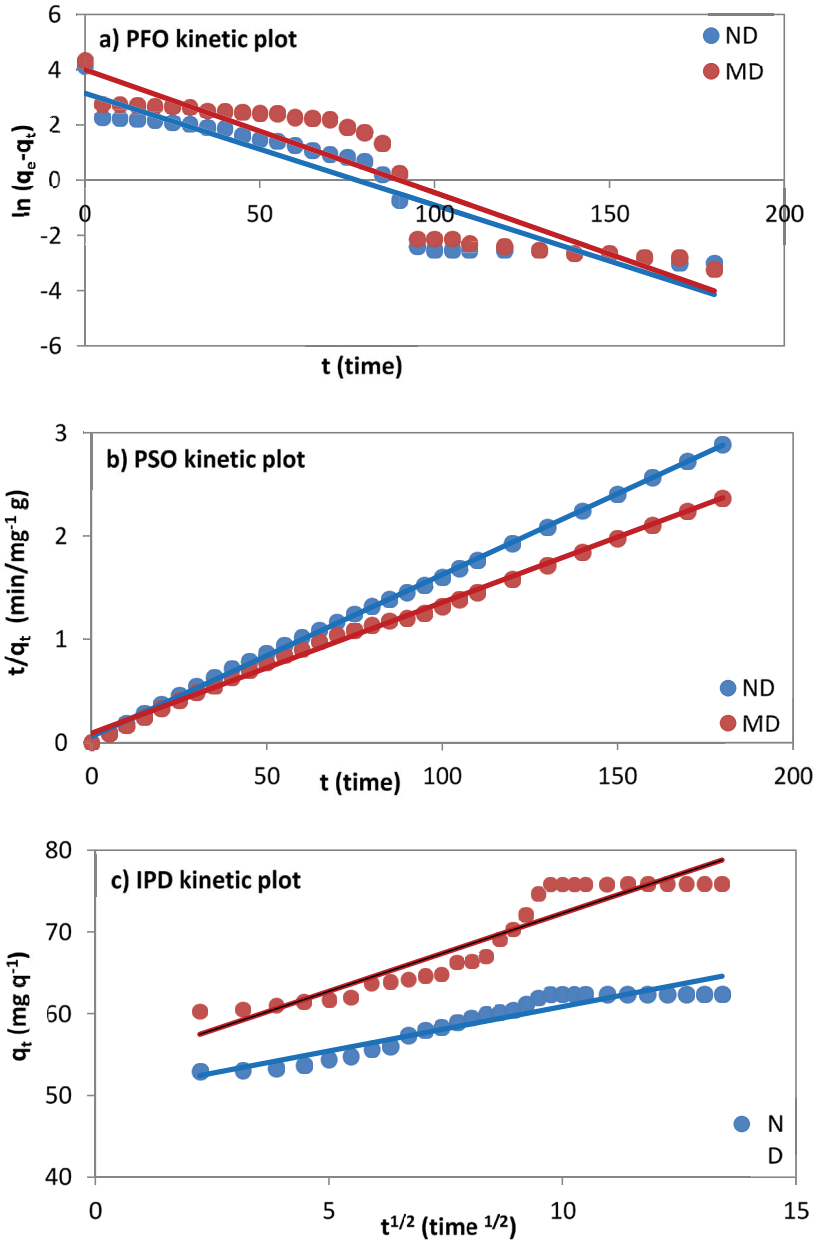

Fig. 5. Kinetic plots of BB 41 adsorption on natural diatomite and modified diatomite: (a) PFO model, (b) PSO model, and (c) IPD model (80 mg L^{-1} initial BB 41 concentration, 318 K).

Table 2
Comparison of BB 41 adsorption capacity of various adsorbents

Adsorbent	Adsorption capacity (mg g^{-1})	Reference
Analcite rich tuff (0.085 mm)	192.31	[31]
Waste brick (WB 1 ± 0.5 mm)	15.00	[32]
Waste brick (Jed-WB)	16.81	
Acid activated montmorillonite	47.12	[33]
Grafted natural adsorbents	7.58, 19.2, 4.9	[34]
Raw fish bone	37.36	[35]
Bituminous shale	26.00	[36]
Juniperus excels shavings powder (JESP)	19.06	[37]
Sodium alginate	12.25	[38]
Raw rice stems	17.70	[39]
Modified rice stems	22.60	
Raw kaolinite	6.21	[40]
Synthetic zeolite (Zeolite X)	17.00	
Date stones activated carbon (DSAC)	13.81	[41]
Salvia seed	19.16	[42]
Pistachio shell	21.83	[43]
Natural diatomite (ND)	56.82	This study
Mn modified diatomite (MD)	85.64	This study

Table 3
Kinetic model parameters for BB 41 adsorption on natural and modified diatomite (initial concentration: 80 mg L^{-1})

Kinetic model	Temperature (K)	Kinetic coefficients	Natural diatomite	Modified diatomite
	298	$q_{e,\exp}$ (mg g^{-1})	55.894	68.032
	308	$q_{e,\exp}$ (mg g^{-1})	61.593	72.551
	318	$q_{e,\exp}$ (mg g^{-1})	62.435	75.953
PFO kinetic model	298	k_1 (min^{-1})	0.0411	0.0447
		$q_{e,\text{cal}}$ (mg g^{-1})	7.6729	43.9301
		R^2	0.8532	0.8638
	308	k_1 (min^{-1})	0.0508	0.0542
		$q_{e,\text{cal}}$ (mg g^{-1})	19.7618	60.2259
		R^2	0.8703	0.8444
	318	k_1 (min^{-1})	0.0539	0.0578
		$q_{e,\text{cal}}$ (mg g^{-1})	28.9102	66.8131
		R^2	0.8841	0.8693
PSO kinetic model	298	k_2 (min^{-1})	0.0495	0.0783
		$q_{e,\text{cal}}$ (mg g^{-1})	56.1798	67.9300
		R^2	0.9999	0.9983
	308	k_2 (min^{-1})	0.0941	0.1525
		$q_{e,\text{cal}}$ (mg g^{-1})	62.8931	71.6268
		R^2	0.9996	0.9982
	318	k_2 (min^{-1})	0.1483	0.1834
		$q_{e,\text{cal}}$ (mg g^{-1})	63.2911	75.7402
		R^2	0.9997	0.9963
IPD kinetic model	298	k_{ipd} (mg g^{-1} $min^{-1/2}$)	0.0231	0.0619
		C (mg g^{-1})	24.949	26.168
		R^2	0.8073	0.8721
	308	k_{ipd} (mg g^{-1} $min^{-1/2}$)	0.0444	0.0637
		C (mg g^{-1})	25.132	28.168
		R^2	0.8376	0.8772
	318	k_{ipd} (mg g^{-1} $min^{-1/2}$)	0.0891	0.0905
		C (mg g^{-1})	49.982	53.231
		R^2	0.9053	0.8864

adsorption on both ND and MD (Table 4). The $\Delta G°$ values decrease as the temperature rises showing that this separation process is better at high temperatures. Accordingly, the increase in dye removal with increasing temperatures is due to chemical bonds, electrostatic interactions, and Van der Waals forces between BB 41 and diatomite. The positive $\Delta H°$ value shows that the removal process is endothermic and the positive $\Delta S°$ value establishes enhanced randomness at the diatomite–dye interface and affinity of diatomite for BB 41 [47]. The Arrhenius plots for BB 41 adsorption on ND and MD are shown in Fig. 6. From these plots, the values of activation energy (E_A) were determined as 42.71 and 58.83 kJ mol^{-1} for BB 41 removal onto ND and MD adsorbents, respectively. The activation energies were higher than 40 kJ mol^{-1} and these values confirm the fact that the process was controlled by chemical adsorption.

3.5. Economic analysis of preparing modified diatomite

The cost of dye removal by an adsorption process is primarily dependent on the cost of the adsorbent. Hence, low-cost or waste materials that are economically more feasible to use and locally available are needed. Diatomite used in this study is an inexpensive and local adsorbent that is available to mine in large amounts. Modification of ND was performed by treatment with $MnCl_2$ and NaOH chemicals with heating and drying processes, respectively. The modification cost for natural diatomite is shown in Table 5 and the total cost for preparation of 1 kg of Mn-modified diatomite

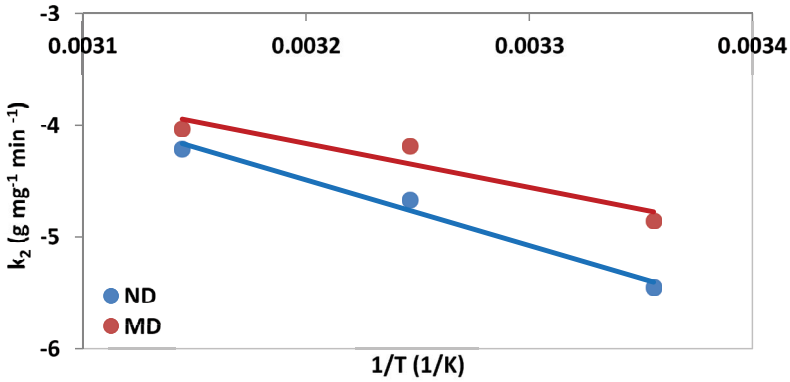

Fig. 6. Arrhenius plots for BB 41 adsorption on natural and modified diatomite.

Table 4
Thermodynamic parameters of BB 41 adsorption on natural and modified diatomite

	Temperature (K)	$\Delta G°$ (kJ mol^{-1})	$\Delta H°$ (kJ mol^{-1})	$\Delta S°$ (J mol^{-1} K^{-1})	R^2
	298	–10.957			
ND	308	–11.091	31.746	133.319	0.9978
	318	–11.224			
	298	–12.171			
MD	308	–13.878	48.706	170.728	0.9964
	318	–15.586			

Table 5
Economic analysis of preparing Mn-modified diatomite

No	Chemicals/outgoings	Unit cost	Amount used	Net cost ($)
1	Sodium hydroxide (NaOH)	80.55 ($/kg)*	0.45 kg	36.25
2	Manganese chloride ($MnCl_2$)	212.55 ($/kg)*	1.05 kg	223.18
3	Hydrochloric acid (HCI)	48.95 ($/L)*	0.35 L	17.13
4	Cost of heating	0.53 kW h^{-1}	0.34 kWh (80°C, 2 h)	0.18
5	Cost of drying	0.53 kW h^{-1}	3.94 kWh (100°C, 24 h)	2.09
6	Net cost			278.83
7	Overhead costs (10% of net cost)			27.88
8	Total cost			306.71

*Cost of chemicals were derived from: https://us.vwr.com/store/product

was obtained as $306.71. In comparison, modified adsorbents such as clays are more costly for small lots. They are however projected to be lower cost in the near future if bulk production methods could be developed and employed.

4. Conclusions

The adsorption of BB 41 on the natural diatomite was investigated under different conditions. The experimental results showed that the removal of BB 41 with natural diatomite increases with dye concentration, contact time, and temperatures. When the initial dye concentration rises from 10 to 80 mg L^{-1}, dye adsorption capacity on ND and MD increases from 6.15 to 62.43 mg g^{-1} and 9.06 to 75.95 mg g^{-1} at 318 K, respectively. Isotherm studies demonstrate that the Freundlich model shows a more suitable profile for BB 41 adsorption on ND and MD than the Langmuir and Temkin models. The parameters of these three isotherms increase as the temperature rises and also indicate that adsorption is more favorable at a higher temperature. The R^2 values of the Freundlich model are higher than the other two models for BB 41 removal with diatomite. Kinetic studies indicate that adsorption of BB 41 follows the PSO model suggests that the rate-limiting step may be dye removal. The thermodynamic parameters indicate that the removal process is endothermic and they suggest feasibility with the spontaneous nature of adsorption on both ND and MD adsorbents. Since the activation energies for this process were higher than 40 kJ mol^{-1}, it confirmed that chemical adsorption was carried out between BB 41 and diatomite. It was determined that natural and modified diatomite have high adsorption capacity for BB 41 and diatomite could be a natural material used for dye removal compared to costly adsorbents.

Acknowledgments

The authors are thanks to Van Yüzüncü Yıl University, Scientific Research Projects Commission (YYÜ BAP) for financial support of this research under the FAP-2019-8601 grant number.

References

[1] D. He, Q. Yu, Y. Liu, X. Liu, Y. Li, R. Liu, J. Xiang, Removal of congo red by magnetic $MnFe_2O_4$ nanosheets prepared via a facile combustion process, J. Nanosci. Nanotechnol., 19 (2019) 2702–2709.
[2] T.B. Pushpa, J. Vijayaraghavan, K. Vijayaraghavan, J. Jegan, Utilization of effective microorganisms based water hyacinth compost as biosorbent for the removal of basic dyes, Desal. Water Treat., 57 (2016) 24368–24377.
[3] M.H. Cui, D. Cui, L. Gao, H.Y. Cheng, A.J. Wang, Analysis of electrode microbial communities in an up-flow bioelectrochemical system treating azo dye wastewater, Electrochim. Acta, 220 (2106) 252–257.
[4] F. Torrades, J.G. Montaño, Using central composite experimental design to optimize the degradation of real dye wastewater by Fenton and photo-Fenton reactions, Dyes Pigm., 100 (2104) 184–189.
[5] X.J. Wu, J.D. Wang, L.Q. Cao, Characterization and adsorption performance of chitosan/diatomite membranes for Orange G removal, e-Polymers, 1 (2016) 99–115.
[6] X. Tao, Y. Wu, H. Sha, Cuprous oxide-modified diatomite waste from the brewery used as an effective adsorbent for removal of organic dye: adsorption performance, kinetics and mechanism studies, Water Air Soil Pollut., 229 (2018) 322–326.
[7] Z. Li, H. Hanafy, L. Zhang, L. Sellaoui, M.S. Netto, M.L.S. Oliveira, M.K. Seliem, G.L. Dotto, A. Bonilla-Petriciolet, Q. Li, Adsorption of congo red and methylene blue dyes on an Ashitaba waste and a walnut shell-based activated carbon from aqueous solutions: experiments, characterization and physical interpretations, Chem. Eng. J., 388 (2020) 124263, doi: 10.1016/j.cej.2020.124263.
[8] P.M. Morais da Silva, N.G. Camparotto, K.T.G. Lira, C.S.F. Picone, P. Prediger, Adsorptive removal of basic dye onto sustainable chitosan beads: equilibrium, kinetics, stability, continuous-mode adsorption and mechanism, Sustainable Chem. Pharm., 18 (2020) 100318, doi: 10.1016/j.scp.2020.100318.
[9] M.R. Abukhadra, F.M. Dardir, M. Shaban, E.A. Ahmed, M.F. Soliman, Superior removal of Co^{2+},Cu^{2+} and Zn^{2+} contaminants from water utilizing spongy Ni/Fe carbonate–fluorapatite; preparation, application and mechanism, Ecotoxicol. Environ. Saf., 157 (2018) 358–368.
[10] M. Shaban, M.R. Abukhadra, A. Hamd, Recycling of glass in synthesis of MCM-48 mesoporous silica as catalyst support for Ni_2O_3 photocatalyst for congo red dye removal, Clean Technol. Environ. Policy, 20 (2108) 13–28.
[11] Y. Wu, X. Li, Q. Yang, D. Wang, Q. Xu, F. Yao, F. Chen, Z. Tao, X. Huan, Hydrated lanthanum oxide-modified diatomite as highly efficient adsorbent for low-concentration phosphate removal from secondary effluents, J. Environ. Manage., 231 (2019) 370–379.
[12] M. Saxena, N. Sharma, R. Saxena, Highly efficient and rapid removal of a toxic dye: adsorption kinetics, isotherm, and mechanism studies on functionalized multiwalled carbon nanotubes, Surf. Interfaces, 21 (2020) 100639, doi: 10.1016/j.surfin.2020.100639.
[13] M.R. Abukhadra, M. Rabia, M. Shaban, F. Verpoort, Heulandite/polyaniline hybrid composite for efficient removal of acidic dye from water; kinetic, equilibrium studies and statistical optimization, Adv. Powder Technol., 29 (2108) 2501–2511.
[14] A.M. Rabie, M. Shaban, M.R. Abukhadra, R. Hosny, S.A. Ahmed, N.A. Negm, Diatomite supported by CaO/MgO nanocomposite as heterogeneous catalyst for biodiesel production from waste cooking oil, J. Mol. Liq., 279 (2109) 224–231.
[15] H.B. Fan, Q.F. Ren, S.L. Wang, Z. Jin, Y. Ding, Synthesis of the Ag/Ag_3PO_4/diatomite composites and their enhanced photocatalytic activity driven by visible light, J. Alloys Compd., 775 (2019) 845–852.
[16] P. Zhu, Y. Chen, M. Duan, M. Liu, P. Zou, Structure and properties of Ag_3PO_4/diatomite photocatalysts for the degradation of organic dyes under visible light irradiation, Powder Technol., 336 (2018) 230–239.
[17] Y. Du, X. Wang, J. Wu, C. Qi, Y. Li, Adsorption and photoreduction of Cr(VI) via diatomite modified by Nb_2O_5 nanorods, Particuology, 40 (2108) 123–130.
[18] Y. Xia, X. Jiang, J. Zhang, M. Lin, X. Tang, J. Zhang, H. Liu, Synthesis and characterization of antimicrobial nanosilver/diatomite nanocomposites and its water treatment application, Appl. Surf. Sci., 396 (2107) 1760–1764.
[19] R.P. Chicinaş, E. Gál, H. Bedelean, M. Darabantu, A. Măicăneanu, Novel metal modified diatomite, zeolite and carbon xerogel catalysts for mild conditions wet air oxidation of phenol: characterization, efficiency and reaction pathway, Sep. Purif. Technol., 197 (2018) 36–46.
[20] H. Lin, X. Wu, J. Zhu, Kinetics, equilibrium, and thermodynamics of ammonium sorption from swine manure by natural chabazite, Sep. Sci. Technol., 51 (2016) 202–213.
[21] M. Sprynskyy, I. Kovalchuk, B. Buszewski, The separation of uranium ions by natural and modified diatomite from aqueous solution, J. Hazard. Mater., 181 (2010) 700–707.
[22] N. Caliskan, A.R. Kul, S. Alkan, E.G. Sogut, İ. Alacabey, Adsorption of Zinc(II) on diatomite and manganese-oxide-modified diatomite: a kinetic and equilibrium study, J. Hazard. Mater., 193 (2011) 27–36.
[23] M. Koyuncu, A.R. Kul, Thermodynamics and adsorption studies of dye (rhodamine-b) onto natural diatomite, Physicochem. Probl. Miner. Process., 50 (2014) 631–643.

[24] S. Alkan, M. Çalişkan, İ. Irende, A.R. Kul, Adsorption equilibrium and thermodynamics of diatomite (Çaldiran/Van) on some textile dyes, J. Chem. Soc. Pak., 40 (2018) 457–466.
[25] I. Langmuir, The adsorption of gases on plane surfaces of glass, mica and platinum, J. Am. Chem. Soc., 40 (1918) 1361–1403.
[26] H. Freundlich, Over the adsorption in solution, J. Phys. Chem., 57 (1906) 385–471.
[27] P.H. Emmett, J.T. Kummer, Kinetics of ammonia synthesis, Ind. Eng. Chem., 35 (1943) 677–683.
[28] S. Lagergren, About the theory of so-called adsorption of soluble substances, Kungl. Svens. Vetenskapsakad. Handl., 24 (1898) 1–39.
[29] Y.S. Ho, G. McKay, Pseudo-second-order model for sorption processes, Process Biochem., 34 (1999) 451–465.
[30] W.J. Weber, J.C. Morris, Kinetics of adsorption on carbon from solutions, J. Sanit. Eng. Div. Proc. Am. Soc. Civ. Eng., 89 (1963) 31–60.
[31] I. Humelnicu, A. Băiceanu, M.E. Ignat, V. Dulman, The removal of Basic Blue 41 textile dye from aqueous solution by adsorption onto natural zeolitic tuff: kinetics and thermodynamics, Process Saf. Environ. Prot., 105 (2017) 274–287.
[32] F. Kooli, Y. Liu, M. Abboudi, H.O. Hassani, S. Rakass, S. Ibrahim, F. Al Wadaani, Waste bricks applied as removal agent of basic blue 41 from aqueous solutions: base treatment and their regeneration efficiency, Appl. Sci., 9 (2019) 11–18.
[33] F. Kooli, Y. Liu, R. Al-Faze, A. Al Suhaimi, Effect of acid activation of Saudi local clay mineral on removal properties of basic blue 41 from an aqueous solution, Appl. Clay Sci., 116–117 (2015) 23–30.
[34] O.G. Allam, N.A. Fathy, M.G. Khafagj, M.K. El-Bisi, Modified waste materials for removal of cationic dye from liquid effluents and their kinetic studies, Egypt. J. Chem., 58 (2015) 141–154.
[35] A. Ebrahimi, M. Arami, H. Bahrami, E. Pajootan, Fish bone as a low-cost adsorbent for dye removal from wastewater: response surface methodology and classical method, Environ. Model. Assess., 18 (2013) 661–670.
[36] A.E. Müftüoglu, B. Karakelle, M. Ergin, A.Y. Erkol, F. Yilmaz, The removal of basic blue 41 dye from aqueous solutions by bituminous shale, Adsorpt. Sci. Technol., 21 (2003) 751–760.
[37] A.R. Kul, A. Aldemir, S. Alkan, H. Elik, M. Caliskan, Adsorption of Basic Blue 41 using *Juniperus excelsa*: isotherm, kinetics and thermodynamics studies, Environ. Res. Technol., 2 (2019) 112–121.
[38] N.M. Mahmoodi, B. Hayati, M. Arami, Kinetic, equilibrium and thermodynamic studies of ternary system dye removal using a biopolymer, Ind. Crops Prod., 35 (2012) 295–301.
[39] A. Akbar, S. Arezomand, H. Reza, A. Hossein, Kinetics and equilibrium studies of the removal of blue basic 41 and methylene blue from aqueous solution using rice stems, Iran. J. Chem. Chem. Eng., 34 (2015) 33–42.
[40] M. Gougazeh, F. Kooli, J.C. Buhl, Removal efficiency of basic blue 41 by three zeolites prepared from natural Jordanian kaolin, Clays Clay Miner., 67 (2019) 143–153.
[41] M.B. Alqaragully, Removal of textile dyes (Maxilon blue, and methyl orange) by date stones activated carbon, Int. J. Adv. Res. Chem. Sci., 1 (2014) 48–59.
[42] A. Hamzezadeh, Y. Rashtbari, S. Afshin, M. Morovati, M. Vosoughi, Application of low-cost material for adsorption of dye from aqueous solution, Int. J. Environ. Anal. Chem., 1 (2020) 1–16.
[43] İ. Şentürk, M. Alzein, Adsorptive removal of basic blue 41 using pistachio shell adsorbent - performance in batch and column system, Sustainable Chem. Pharm., 16 (2020) 100254, doi: 10.1016/j.scp.2020.100254.
[44] S. Archin, S.H. Sharifi, G. Asadpour, Optimization and modeling of simultaneous ultrasound-assisted adsorption of binary dyes using activated carbon from tobacco residues: response surface methodology, J. Cleaner Prod., 239 (2019) 118136, doi: 10.1016/j.jclepro.2019.118136.
[45] M.T. Yagub, T.K. Sen, S. Afroze, H.M. Ang, Dye and its removal from aqueous solution by adsorption: a review, Adv. Colloid Interface Sci., 209 (2014) 172–184.
[46] V.K. Gupta, Suhas, Application of low-cost adsorbents for dye removal–a review, J. Environ. Manage., 90 (2009) 2313–2342.
[47] P.R. Souza, G.L. Dotto, N.P.G. Salau, Experimental and mathematical modeling of hindered diffusion effect of cationic dye in the adsorption onto bentonite, J. Environ. Chem. Eng., 7 (2019) 1–7.